Research Article Open Access

Lingnan Kong, Yaohui Liu, Jia'an Liu, Yulai Song*, Shasha Li, Yan Liang, Yi Zheng, and Wei Cui

Kinetics of the austenitization in the Fe-Mo-C ternary alloys during continuous heating

DOI 10.1515/phys-2016-0078 Received May 30, 2016; accepted Dec 12, 2016

Abstract: The influence of molybdenum on the microstructure and kinetics of the austenization of the Fe-Mo-C ternary alloys is analyzed using differential scanning calorimetry (DSC) and the Johnson-Mehl-Avrami-Kolmogorov model (JMAK) in the temperature range from 293 K to 1373 K. The as-cast microstructure and microstructure after DSC test are obtained using optical microscopy (OM) and scanning electron microscopy (SEM). It was seen that with an increasing Mo concentration, the lamellar pearlite is spherized and the austenite grain size decreases. In addition, both DSC curves and the JMAK model show that the initial (Ac1) and the final (Ac3) temperature of the phase transition increases with an increasing Mo concentration. It was also seen that increasing the Mo concentration, the diffusion activation energy (DAE) increases and the pre-exponential factor of diffusion (DPEF) decreases due to a change in both the austenitic nucleation rate and the diffusion of the elements caused by the introduction of Mo.

Keywords: General theory of phase transitions; Metals and alloys; Dynamics and criticality; Phase separation and segregation in alloying

PACS: 64.60.Bd; 64.70.kd; 64.70.qj; 64.75.Op

1 Introduction

In the annealing, quenching and other heat treatment process, steels are frequently processed into the austenite state to obtain the expected organization and performance. Thus, the formation of the high temperature austenitic phase is a very important processes [1, 2] It is well known that the chemical composition and the final microstructure determine the mechanical properties of steels. For steels, the mechanical properties are completely determined by its microstructure when the chemical composition has been confirmed. Moreover, the final microstructure, depending on the austenite formation, determines its mechanical properties [3–5]. Some reports indicate that acicular ferrite is easier to form when the austenitic grain size reaches a critical state [6, 7]. Lee et al. [8] found that a reduced austenite grain size results in a decrease of the bainite transformation temperatures (Bs and Bf). Thus, the selection of appropriate heat treatment parameters based on the austenitization process is the only way to obtain the expected microstructure [9, 10]. However, because the kinetics of austenitization has not attracted significant attention, there is minimal information regarding the kinetics of austenite transformation for cases other than the decomposition of austenite [11-13].

In addition to the heat treatment, the chemical composition also affects the final microstructure and mechanical properties of steels [14]. In recent years, it is one of the main ways that the additional elements are doped into steels to improve their mechanical properties [15–17]. Meanwhile the introduction of additional elements also has an impact on the austenitization process. The research on the austenitization process of martensite in Fe-C-M alloys, found that the kinetics of austenitization may change by the introduction of alloying elements [18]. However, there is currently no systematic study for the influence of the introduction of additional elements on the pearliteto-austenite transformation process, in addition to Speich and Szirmae, who reported that the addition of Mn, Si and Cr can slow down the pearlite-austenitic phase transition [19]

^{*}Corresponding Author: Yulai Song: Key Laboratory of Automobile Materials of Ministry of Education & School of Materials Science and Engineering, Nanling Campus, Jilin University, No. 5988 Renmin Street, Changchun 130025, PR China; Email: songyulai2005@163.com; Tel.: +86 0431 85095862; Fax: +86 0431 85095862 Lingnan Kong, Yaohui Liu, Jia'an Liu, Shasha Li, Yan Liang, Yi Zheng, Wei Cui: Key Laboratory of Automobile Materials of Ministry of Education & School of Materials Science and Engineering, Nanling Campus, Jilin University, No. 5988 Renmin Street, Changchun 130025, PR China

In this paper, the influence of Mo on the kinetics of the austenitization process is studied. A phase transformation model has been adopted to calculate the austenite fraction. The result should contribute to a deeper understanding of the kinetics of austenitization process of carbon steel.

2 Experimental

2.1 Preparation of test specimens

Fe-Mo-C ternary alloys containing three sets of Mo concentration were smelted by an intermediate frequency furnace at 1873 K and poured into a Y-shaped mold. The small amounts of Al were added before the molten steel was poured to remove the oxygen. After cooling to room temperature, the ingot quality is close to 5 kg. The chemical composition is shown in Table 1.

Table 1: Chemical composition of the samples (wt.%)

| | С | Мо | S | Р | Fe |
|----|------|------|------|------|------|
| 1# | 0.87 | 0.17 | 0.03 | 0.04 | Bal. |
| 2# | 0.88 | 0.45 | 0.03 | 0.03 | Bal. |
| 3# | 0.89 | 0.59 | 0.03 | 0.03 | Bal. |

2.2 Differential scanning calorimetry (DSC)

In order to study the austenitization process, each of the three specimens were processed into a cylindrical shape with a size of Φ 2.0–0.5 mm, which was used to perform the DSC experiments by a Netzsch DSC 404C. The experimental temperature was increased from 293 K to 1373 K at 10 K/min, then immediately cooled down to 293 K at 40 K/min. Moreover, the experiments were executed under a high pure flowing argon protection.

2.3 Metallographic structure

For the casting structure of the specimens, a cube with a size of 10 mm was selected from an ingot in the same location, and the specimens was rubbed, polished, and corroded by 5% Nital to obtain the casting structures by scanning electron microscopy.

In order to obtain the austenite nucleation density, specimens with a size of 10 mm were heated at 10 K/min

to 10 K above Ac1 from room temperature, and then water-quenched to room temperature. After polishing, the grain boundaries were corroded with a solution of picric acid and sodium dodecyl benzene sulfonate (SDBS). The optical microscopy was employed to study the structures. The statistics for the size of the austenite grain were obtained through the line-intercept method in the optical micrographs [20].

3 Results and discussion

3.1 Microstructure analysis

Fig. 1 shows the as-cast microstructure of the specimens, which predominantly consists of pearlite. It should be noted that the structure of pearlite changes from a fine lamellar to a spheroidal shape with an increased Mo concentration.

As is known, when the growth rate of the lamellar pearlite is slower than that of the divorced pearlite, there will be a morphology transformation between the two kinds of pearlite [21]. In addition, the divorced eutectoid transformation is not only related with the low cooling rate, but it is also related to the pre-existing cementite particles, such as when the carbide spacing and undercooling are very small, it will be prone to divorced eutectoid transformation [22, 23]. In the phase diagram of Fe-Mo-C, the proeutectoid carbide M₆C and M₃C would precipitate in the austenite matrix during cooling when the concentration of carbon is higher than 1 wt.%. Moreover, the Mo element is a strong ferrite stabilizer in steel, the A1 temperature will slightly increase after the introduction of Mo in steel. This means that the undercooling of pearlite transformation increases with Mo concentration increase under the same conditions (in the sandbox), which is not conducive to divorced pearlite transformation. That is to say, the morphology transformation between the two kinds of pearlite occurred under the coaction of above two factors.

Fig. 2 illustrates the OM images for all specimens after austenitization process. The images show the typical prior austenitic grain boundaries. The thick black lines are the grain boundaries in the images, and the measurement results of average grain size are given in Table 2. The austenitic sizes decrease with a concentration increase of Mo. The results confirm earlier experiments in which the austenite grain size was refined by adding the alloying elements into steels [24]. Moreover, there are carbides (red circles) at the grain boundaries, and the number increases with an increase in Mo concentration. The carbides not

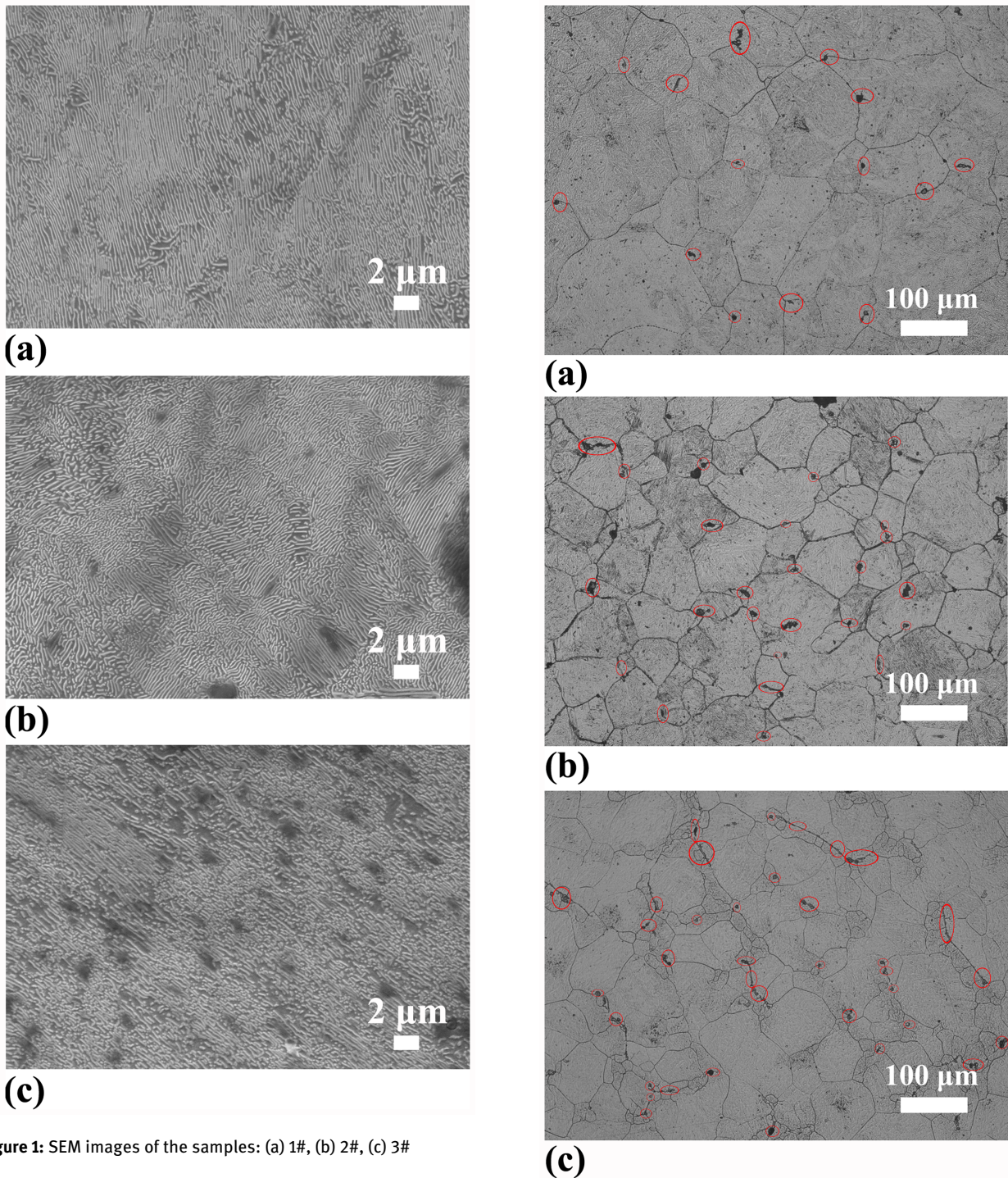


Figure 1: SEM images of the samples: (a) 1#, (b) 2#, (c) 3#

only produce more nucleation sites, but also have a pinning effect to prevent the growth of anstenite. Thus, the size of the austenite grain is smaller with an increase in Mo concentration.

In the case of initial nucleation, austenitic transformation can be assigned to the site saturation model, therefore the quantity of the new particles formed is not changed at the nucleation site during the austenitization process [25].

Figure 2: Optical micrographs of the samples: (a) 1#, (b) 2#, (c) 3#

Assuming a cubic growth, the geometry factor (g) is 1 [26]. Thus the number of nucleation per unit volume (N^*) can be obtained by $N^* = 1/d^3$, where *d* denotes the grain sizes in Table 2.

Table 2: The average austenite grain size (d) and the estimated nucleus density (N^*) of the samples

| | 1# | 2# | 3# |
|-----------------------------|-----------------------|-----------------------|-----------------------|
| <u>d</u> (μm) | 70.86 | 59.15 | 38.83 |
| $N^{\star} ({\sf m}^{-3})$ | 2.81×10 ¹² | 4.83×10 ¹² | 1.71×10 ¹³ |

3.2 DSC analysis

Fig. 3 shows the classic DSC spectra. Clear endothermic peaks confirm the pearlite-austenite phase transition in thee spectra. The corresponding values of the initial (Ac1) and the final temperature (Ac3) of phase transition are provided in Table 3. As shown in the DSC spectra, it is seen that the exothermic peak has moved to the higher temperature as the Mo concentration increases, indicating that the resistance of the phase transition becomes larger with the introduction of Mo.

Table 3: The onset temperature (Ac1) and the end temperature (Ac3) for the transformation of the samples

| | 1# | 2# | 3# |
|---------|---------|---------|---------|
| Ac1 (K) | 1010.55 | 1015.59 | 1017.21 |
| Ac3 (K) | 1025.43 | 1031.08 | 1035.34 |

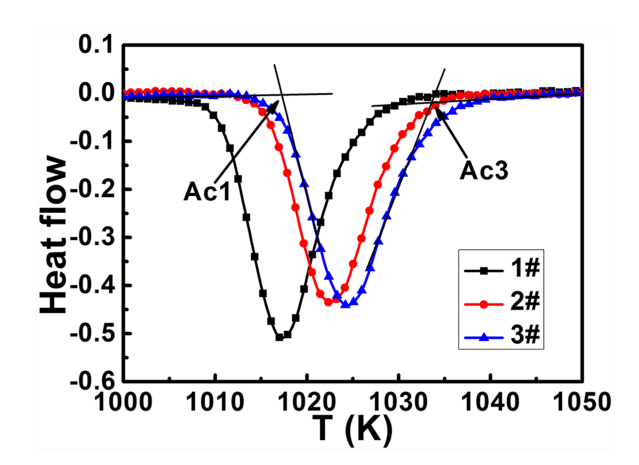


Figure 3: DSC curves of the samples

Generally speaking, according to the DSC spectra, a set of transformation curves can be obtained for the transformation kinetics: the transition fractions are plotted as a function of time or temperature, respectively [27]. In this case, the heating rate is constant, belonging to the isochronal experiment. Thereby, the transformation process can be described by the JMAK models. In the JMAK

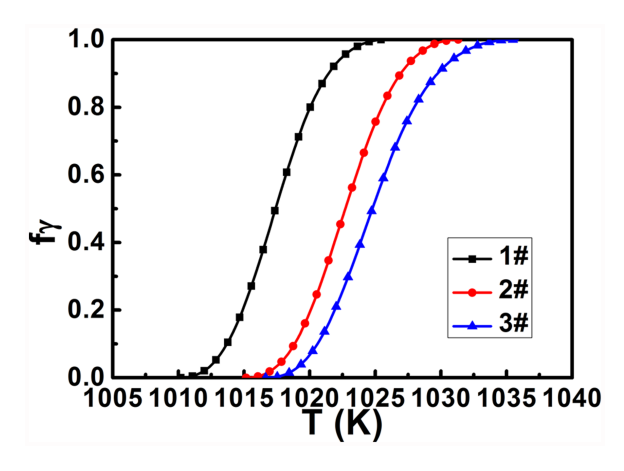


Figure 4: The austenite fraction as a function of temperature calculated from DSC measurements

model, when the temperature is T, the relationship between the transition fraction and the time can be expressed as

$$f\gamma(t) = (1/\Delta HA) \int_{0}^{T} Fu(t)dt$$
 (1)

where Fu is the heat flux and ΔHA is the total change in enthalpy of austenitization process.

The transition fractions are plotted as a function of temperature for various Mo concentrations in Fig. 4. it can be seen that the curve is S-shaped, which shows that the austenitization process of all specimens exhibit the same kinetic features, which can be attributed to the same types of phase transition [28]. Moreover, the values of the phase transition temperature increase significantly as the Mo concentration increases.

The transformation rate curves, df_{γ}/dt with respect to temperatures and the transformed fraction, obtained for the different Mo concentration, are shown in Fig. 5a and Fig. 5b, respectively. They exhibit the following (kinetic) features:

- (i) It appears that the values of the initial and final temperature of austenitization rise as the Mo concentration increases (Table 3 and Fig. 5a).
- (ii) The time required for phase transformation slightly increases as Mo concentration increase (Ac3-Ac1), as shown in Figs. 5a.
- (iii) There is only one austenite formation rate maximum in Fig. 5, and decreases as the Mo concentration increases, indicating that a same types of phase transition takes place in all specimens [28].

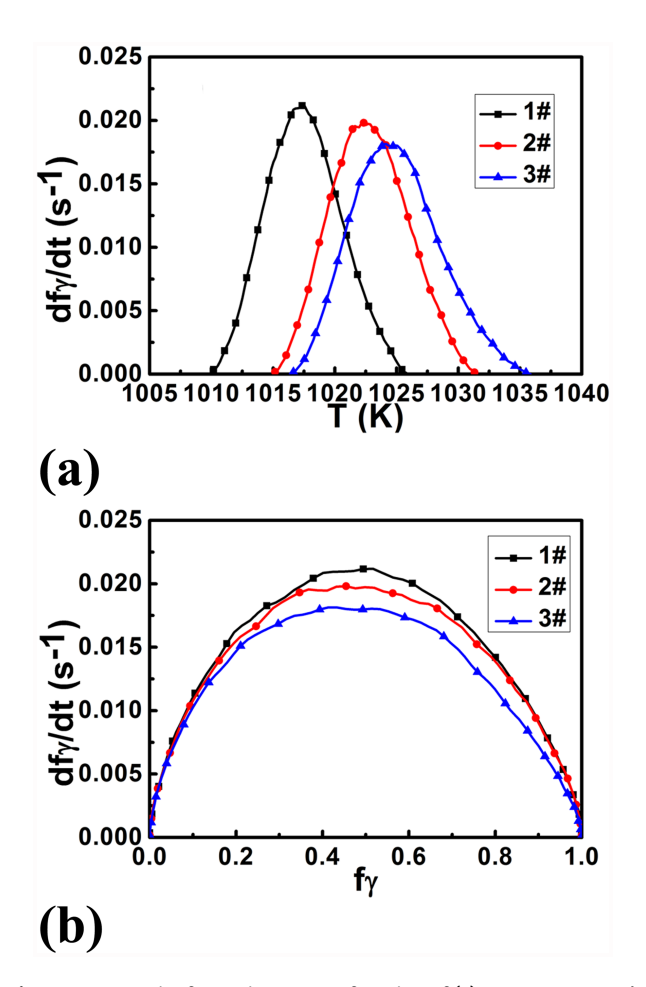


Figure 5: Austenite formation rate as function of (a) temperature and (b) austenite fraction of the samples

3.3 Kinetics

In the JMAK models, to study the transformation kinetics, the modes of nucleation, growth and the impingement correction must be definite. Based on classical nucleation theory, there are fluctuations in energy, microstructure and composition at the interfaces between ferrite and cementite, which causes the nucleation of austenite produces preferentially at the interface [24]. Because of austenite transformation can be classified as the site saturation model, the nucleation rate, $\stackrel{\circ}{N}$, can be described as [12]

$$\stackrel{\circ}{N} = N^* \delta(t - 0) \tag{2}$$

where $\delta(t-0)$ is the Dirac delta function:

$$\delta(t-0) = \begin{cases} 0(t \neq 0) \\ \infty(t=0) \end{cases}, \quad \int_{-\infty}^{\infty} \delta(t-0)dt = 1$$
 (3)

In the site nucleation model, it can be assumed that the number of the nucleation remains unchanged at the beginning of growth. Hence, the Dirac delta function is 1, so $\stackrel{\circ}{N} = N^{\star}$.

The expanded volume fraction, as an adaptive way, is used in the connection between nucleation, growth, and impingement in the modularization method. In the growth process, it is assumed that second-phase particles could separate the nucleation and growth. The expanded transformed volume fraction, x_e , is written as

$$x_e(t) = \int_0^t \mathring{N}.(\tau)Y(t,\tau)d\tau \tag{4}$$

where *Y* is the volume of new particles. The volume is calculated according to the following equation:

$$Y(t,\tau) = g(\int_{\tau}^{t} v(T)dt)^{d/m}$$
 (5)

where g is the geometry factor (for cubic or spherical growth, g = 1 and $g = 4\pi/3$, respectively); d is the growth dimensionality; m is the growth parameter (when interface or volume diffusion controlled growth m = 1 and m = 2, respective); the growth velocity is obtained by following equation:

$$v(T) = v_0 \exp(-\frac{Q_G}{RT}) \tag{6}$$

where v_0 denotes the pre-exponential factor (GPEF) and Q_G is the activation energy of growth (GAE). Thereby, the model of nucleation and growth can be configured to the rate controlled by the activation energy. In case of the growth of austenite belongs to the diffusion-controlled growth, $v_0 = D_0$ and $Q_G = Q_d$, where D_0 and Q_d are DPEF and DAE, respectively [29].

In the JMAK model, a hypothesis is applied that all particles always grow and new particles also nucleate, in other words, the impingement between particles is not considered in the calculation process of the particle volume. It means that there are differences between the expanded and the sincere volume. Thus, the expanded volume must be redressed, so the expanded volume, V^e , can be found as

$$V^{e} = \int_{0}^{t} V \stackrel{\circ}{N} Y(t, \tau) d\tau$$
 (7)

where V is the specimens volume. On the basis of Eq. (2) and Eqs. (5)–(7), the expanded volume is described as:

$$V^{e} = \int_{T_{0}}^{T(t)} V N^{*} \delta \left(\frac{T(\tau) - T_{0}}{\Phi} \right)$$
 (8)

700 — L. Kong et al. DE GRUYTER OPEN

$$\cdot g \left(\int_{T(\tau)}^{T(t)} D_0 \exp\left(-\frac{Q_d}{RT}\right) d\frac{T}{\Phi} \right)^{3/2} d\frac{T(\tau)}{\Phi}$$

where Φ is the heating rate. An improved approximation of the temperature integral has to be adopted to reduce the error caused by the integral during the deduction of analytical modular phase transformation model [30]. Especially, when the transformation is fast, the approximate equation can be written as:

$$\int_{T(\tau)}^{T(t)} \exp\left(-\frac{Q_d}{RT}\right) dT \approx \exp\left(-\frac{Q_d}{RT(t)}\right)$$

$$\cdot \int_{T(\tau)}^{T(t)} \exp\left(\frac{Q_d(T - T(t))}{RT(t)^2}\right) dT$$

$$= \exp\left(-\frac{Q_d}{RT(t)}\right) \frac{RT(t)^2}{Q_d} \left(1 - \exp\left(\frac{Q_d(T(\tau) - T(t))}{RT(t)^2}\right)\right)$$

According to Eq. (9) and Eq. (8) can be obtained:

$$V^{e} = VN^{*}g \left(\frac{D_{0}}{\Phi}\right)^{3/2} \left(\exp\left(-\frac{Q_{d}}{RT(t)}\right) \frac{RT(t)^{2}}{Q_{d}} \right) \cdot \left(1 - \exp\left(\frac{Q_{d}(T_{0} - T(t))}{RT(t)^{2}}\right)\right)^{3/2}$$

Finally, the impingement correction with following equation

$$\frac{df_{\gamma}}{dx_e} = (1 - f_{\gamma}) \tag{11}$$

where x_e is defined as V^e/V , and, after integration

$$f_{\gamma} = \frac{V_t}{V} = 1 - \exp\left(-\frac{V^e}{V}\right) \tag{12}$$

On the basis of Eq. (10) and Eq. (12), the austenite fraction is expressed as:

$$f_{\gamma} = 1 - \exp\left(-N^{\star}g(\frac{D_0}{\Phi})^{3/2} \left(\exp\left(-\frac{Q_d}{RT(t)}\right)\right)$$

$$\frac{RT(t)^2}{Q_d} \left(1 - \exp\left(\frac{Q_d(T_0 - T(t))}{RT(t)^2}\right)\right)^{3/2}$$
(13)

In Eq. (13), it is worth mentioning that the equation lacks D_0 and Q_d , before obtaining the final results of calculated austenite fraction. Thus according to Eq. (13), the experimental data is fitted with the calculated data from the JMAK model, and then the values of D_0 and Q_d are obtained and presented in Table 4, which are consistent with previous results [31, 32].

Table 4: Kinetic parameters determined using the phase-transformation model of the samples

| 1# | 2# | 3# |
|-----------------------|--------------------------------|--|
| 82.66 | 89.73 | 96.38 |
| | | |
| 1.57×10^{-9} | 1.32×10^{-9} | 1.21×10^{-9} |
| 1.4 | 1.2 | 1.3 |
| | 82.66 1.57×10 ⁻⁹ | 82.66 89.73 1.57×10 ⁻⁹ 1.32×10 ⁻⁹ |

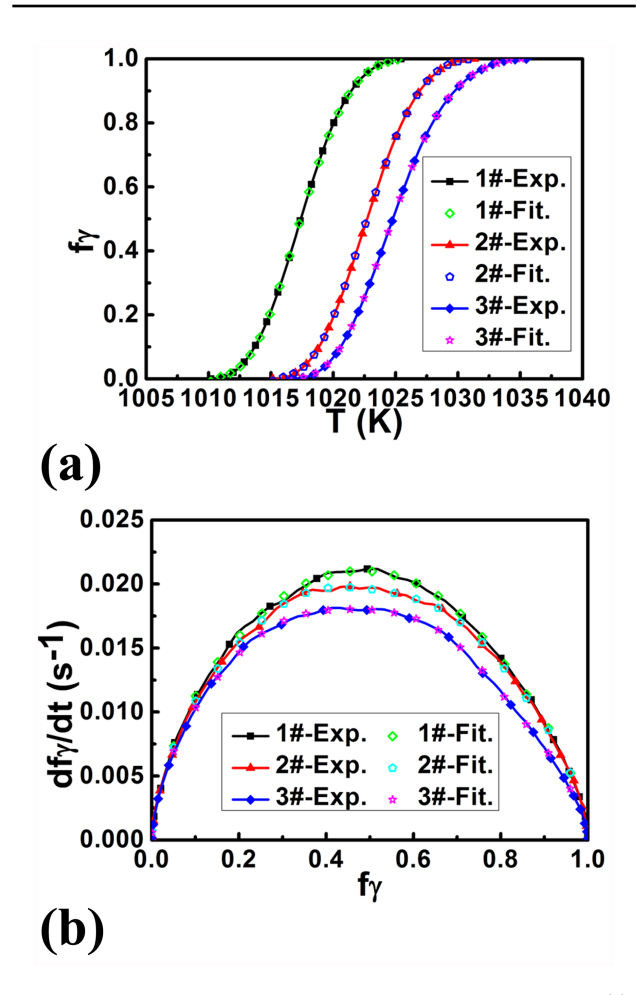


Figure 6: Comparison between measured and calculated values: (a) the relationship between the austenite fraction $(f\gamma)$ and temperature; (b) the relationship between the austenite fraction $(f\gamma)$ and the formation rate

Fig. 6 shows the comparison between the experimental and the fitted curve of the austenite fraction with respect to temperature (Fig. 6a) and formation rate (Fig. 6b), respectively. It can be seen that the two curves are broadly consistent.

The formation of austenite is related to the interface movement by diffusion. According to the Eq. (13), the diffusion process is affected by temperature, DPEF and DAE. The three parameters are affected by the external conditions such as heat, pressure and stress, and internal factors such as organization, structure and chemical composition.

In this study, the phase transition temperature is increased with Mo addition, which means that the phase transition occurs at a higher temperature range. Since the austenitic phase transformation follows diffusion model transformation, and higher temperature can accelerate the diffusion rate of element, it is advantageous to the austenite growth.

However, austenitic phase transformation is not only affected by temperature, but also by structure. With the increase in Mo concentration, the original dense lamellar pearlite structure is gradually transformed into the mixture of spheroidal and lamellar pearlite, and the proportion of spheroidal pearlite increases. The change leads to a decrease in the number of interfaces between the ferrite and cementite. The inhomogeneous distribution of carbon and the irregular atomic arrangement in the interfaces between ferrite and cementite may lead to the fluctuations of structure, energy and concentration. These fluctuations are beneficial to the nucleation of austenite, which often occurs at the interfaces. Thus, the reduction of the interfaces between ferrite and cementite causes the reduction in austenite nucleation sites. In addition, the diffusion of carbon controls the austenitic growth, accordingly the finer pearlite lamellar spacing can shorten the effective diffusion distance of carbon. Therefore, the change of the original structure caused by the addition of Mo is unfavorable for the nucleation of austenite and diffusion of carbon in austenite and decreases the formation rate of austenite. It will reduce diffusion coefficient of carbon, and increase the overall transformation time.

The chemical composition also affects the austenitic phase transformation. Mo element belong to carbide forming element, its carbide is stable and insoluble [33]. It means that carbon activity gradient is changed at the interfaces of austenite/cementite/ferrite. Thus, the coefficient of diffusion and the formation rate of austenite decreases.

Higher temperature increases the diffusion coefficient, and shortens the transformation time. However, the difference between the three groups of temperature (Ac1) is relatively small. Therefore, the influence of temperature is not obvious compared to the microstructure and chemical composition. Thus, the pre-exponential factors of diffusion decrease with the increase in Mo content under the action of the three aspects.

4 Conclusions

The influence of Mo on the microstructure and the kinetics of the austenitization of the Fe-Mo-C ternary alloys are investigated. The analysis indicates that:

- (i) The beginning and the finishing temperature of the hase transition rise with Mo concentration.
- (ii) The austenitization process can be distinguished in three steps: site nucleation, diffusion-controlled growth, and impingement correction.
- (iii) Mo reduces the diffusion coefficient of carbon, thus inhibits the diffusion-controlled austenitic transformation and increases the transformation time.
- (iv) The pre-exponential factor (DPEF) and the activation energy of diffusion (DAE) decrease and increase with Mo concentration increase, respectively.

Acknowledgement: This work is supported by the National Natural Science Foundation of China (Grant No.51201068, No, 50901035), the Science and Technology Development Projects of Jilin Province (Grant No. 20130301006GX, No. 20140101051JC and No. 20130204017GX).

References

- Isfahany A.N., Saghafian H., Borhani G., The effect of heat treatment on mechanical properties and corrosion behavior of AISI420 martensitic stainless steel, J. Alloys Compd., 2011, 509, 3931-3936.
- [2] Zhang Z., Wang Z., Jiang Y., Tan H., Han D., Guo Y., et al., Effect of post-weld heat treatment on microstructure evolution and pitting corrosion behavior of UNS S31803 duplex stainless steel welds, Corros. Sci., 2012, 62, 42-50.
- [3] Bouaziz O., Allain S., Scott C., Cugy P., Barbier D., High manganese austenitic twinning induced plasticity steels: A review of the microstructure properties relationships, Curr. Opin. Solid State Mater. Sci., 2011, 15, 141-168.
- [4] Sun J., Yu H., Wang S., et al., Study of microstructural evolution, microstructure-mechanical properties correlation and collaborative deformation-transformation behavior of quenching and partitioning (Q&P) steel, Mater. Sci. Eng. A, 2014, 596, 89-97.
- [5] Jiménez J.A., Frommeyer G., Analysis of the microstructure evolution during tensile testing at room temperature of highmanganese austenitic steel, Mater. Charact., 2010, 61, 221-226.
- Lee J., Pan Y., Microstructure and toughness of the simulated heat-affected zone in Ti-and Al-killed steels, Mater. Sci. Eng. A, 1991, 136, 109-119.
- Thewlis G., Transformation kinetics of ferrous weld metals, Mater. Sci. Technol., 1994, 10, 110-125.
- Lee S.J., Park J.S., Lee Y.K., Effect of austenite grain size on the transformation kinetics of upper and lower bainite in a low-alloy

- steel, Scr. Mater., 2008, 59, 87-90.
- [9] Jaasona K., Peetsalua P., Saarnaa M., Kulua P., Miklia V., Linda L., et al., Influence of steel austenitization to part quality in continuous austempering, Est. J. Eng., 2012, 18, 221-231.
- [10] Gao Q., Liu Y., Di X., Dong Z., Yan Z., The isochronal $\delta \to \gamma$ transformation of high Cr ferritic heat-resistant steel during cooling, I. Mater. Sci., 2011, 46, 6910-6915.
- [11] Lan L., Qiu C., Zhao D., Gao X., Du L., Effect of reheat temperature on continuous cooling bainite transformation behavior in low carbon microalloyed steel, J. Mater. Sci., 2013, 48, 4356-
- [12] Liu Y., Wang D., Sommer F., Mittemeijer E.J., Isothermal austenite-ferrite transformation of Fe-0.04 at.% C alloy: Dilatometric measurement and kinetic analysis, Acta Mater., 2008, 56, 3833-3842.
- [13] Zhang D., Terasaki H., Komizo Y.i., In situ observation of phase transformation in Fe-0.15 C binary alloy, J. Alloys Compd., 2009, 484, 929-933.
- [14] Alexopoulos N.D., Low-alloy TRIP steels: Evaluation of the mechanical performance with regard to material design requirements in the automotive industry, Steel Res. Int., 2006, 77, 129-138.
- [15] Dumay A., Chateau J. P., Allain S., Migot S., Bouaziz O., Influence of addition elements on the stacking-fault energy and mechanical properties of an austenitic Fe-Mn-C steel. Mater. Sci. Eng. A. 2008, 483, 184-187.
- [16] Chung R., Tang X., Li D., Hinckley B., Dolman K., Microstructure refinement of hypereutectic high Cr cast irons using hard carbide-forming elements for improved wear resistance, Wear, 2013, 301, 695-706.
- [17] Zhi X., Liu J., Xing J., Ma S., Effect of cerium modification on microstructure and properties of hypereutectic high chromium cast iron, Mater. Sci. Eng. A, 2014, 603, 98-103.
- [18] Miyamoto G., Usuki H., Li Z.D., Furuhara T., Effects of Mn, Si and Cr addition on reverse transformation at 1073K from spheroidized cementite structure in Fe-0.6 mass% C alloy, Acta Mater., 2010, 58, 4492-4502.
- [19] Speich G., Szirmae A., Richards M., Formation of austenite from ferrite and ferrite-carbide aggregates, Trans. Met. Soc. Aime., 1969, 245, 1063-1074.
- [20] Huo J., Liu Y., Zhang D., Yan Z., Gao Z., Isochronal phase transformations of low carbon high strength low alloy steel upon continuous cooling, Steel Res. Int., 2013, 84 184-191.

- [21] Verhoeven J.D., Gibson E.D., The divorced eutectoid transformation in steel, Metall. Mater. Trans. A, 1998, 29, 1181-1189.
- [22] Pandit A., Bhadeshia H., Divorced pearlite in steels, In Proc. R. Soc. A, The Royal Society, 2012, 468, 2767-2778.
- [23] Luo D., Peet M., Ooi S., Yan P., Yin Z., Bhadeshia H., Spheroidisation of hypereutectoid state of nanostructured bainitic steel, Mater. Sci. Technol., 2014, 30, 1282-1286.
- [24] Kong L.N., Liu Y.H., Liu J.A., Song Y.L., Li S.S., Zhang R.H., et al., The influence of chromium on the pearlite-austenite transformation kinetics of the Fe-Cr-C ternary steels, J. Alloys Compd., 2015, 648, 494-499,
- [25] Liu C., Liu Y., Zhang D., Yan Z., Kinetics of isochronal austenization in modified high Cr ferritic heat-resistant steel, Appl. Phys. A, 2011, 105, 949-957.
- [26] Hong S.C., Lim S.H., Hong H.S., Lee K.J., Shin D.H., Lee K.S., Effects of Nb on strain induced ferrite transformation in C-Mn steel, Mater. Sci. Eng. A, 2003, 355, 241-248.
- [27] Rheingans B., Mittemeijer E., Phase transformation kinetics: advanced modeling strategies, JoM, 2013, 65, 1145-1154.
- [28] Liu Y., Sommer F., Mittemeijer E., Abnormal austenite-ferrite transformation behaviour in substitutional Fe-based alloys, Acta Mater., 2003, 51, 507-519.
- [29] Ma Q., Shao Y., Liu Y., Gao Z., Yu L., Martensite-austenite transformation kinetics of high Cr ferritic heat-resistant steel, Int. J. Mater. Res., 2013, 104, 935-940.
- [30] Wang D., Liu Y., Zhang Y., Improved analytical model for isochronal transformation kinetics, J. Mater. Sci., 2008, 43, 4876-4885.
- [31] Liu Y., Sommer F., Mittemeijer E., Austenite-ferrite transformation kinetics under uniaxial compressive stress in Fe-2.96 at.% Ni alloy, Acta Mater., 2009, 57, 2858-2868.
- [32] Liu Y., Sommer F., Mittemeijer E., Kinetics of austenitization under uniaxial compressive stress in Fe-2.96 at.% Ni alloy, Acta Mater., 2010, 58, 753-763.
- [33] Zhang H., Pradeep K.G., Mandal S., Ponge D., Raabe D., New insights into the austenitization process of low-alloyed hypereutectoid steels: Nucleation analysis of strain-induced austenite formation, Acta Mater., 2014, 80, 296-308.